A stochastic approach to estimate intraocular pressure and dynamic corneal responses of the cornea

Yaghoubi, Vahid; Setayeshnasab, Hamed; Mosaddegh, Peiman; Kadkhodaei, Mahmoud

DOI
10.1016/j.jmbbm.2022.105210

Publication date
2022

Document Version
Final published version

Published in
Journal of the Mechanical Behavior of Biomedical Materials

Citation (APA)
Yaghoubi, V., Setayeshnasab, H., Mosaddegh, P., & Kadkhodaei, M. (2022). A stochastic approach to estimate intraocular pressure and dynamic corneal responses of the cornea. *Journal of the Mechanical Behavior of Biomedical Materials*, *130*, Article 105210. https://doi.org/10.1016/j.jmbbm.2022.105210

journal of the mechanical behavior of biomedical materials 130 (2022) 105210

Contents lists available at ScienceDirect

Journal of the Mechanical Behavior of Biomedical Materials

journal homepage: www.elsevier.com/locate/jmbbm

A stochastic approach to estimate intraocular pressure and dynamic corneal responses of the cornea

Vahid Yaghoubi [a,b,*], Hamed Setayeshnasab [a], Peiman Mosaddegh [a], Mahmoud Kadkhodaei [a]

[a] Department of Mechanical Engineering, Isfahan University of Technology, Isfahan, 84156-83111, Iran
[b] Structural Integrity & Composites, Faculty of Aerospace Engineering, Delft University of Technology, 2629 HS, Delft, Netherlands

ARTICLE INFO

Keywords:
Corneal biomechanics
IOP estimation
CorVis ST
Finite element modeling
Stochastic modeling
Sensitivity analysis

ABSTRACT

IntraOcular Pressure (IOP) is one of the most informative factors for monitoring the eye-health. This is usually measured by tonometers. However, the outputs of the tonometers depend on the physical and geometrical properties of the cornea. Therefore, the common practice is to develop a numerical model to generate some correction factors. The main challenge here is the accuracy and efficiency of a numerical model in predicting the IOP and Dynamic Corneal Response (DCR) of each patient. This study addresses this issue by developing a two-step surrogate model based on adaptive sparse Polynomial Chaos Expansion (PCE) for fast and accurate prediction of the IOP. In this regard, first, an FE model of the cornea has been developed to predict the DCR parameters. This FE model has been replaced with a PCE-based surrogate model to speed up the simulation step. The uncertainties in the geometry and material model of the cornea have been propagated through the surrogate model to estimate the distributions of the DCR parameters. In the second step, the combination of DCR parameters and the input parameters provide a proper parameter space for developing an efficient data-driven PCE model to predict the IOP. Moreover, sensitivity analysis by using PCE-based Sobol indices has been performed. The results demonstrate the accuracy and efficiency of the proposed method in predicting the IOP. Sensitivity analysis revealed that IOP measurement was influenced mostly by deflection amplitude and applanation time. The analysis indicates the importance of the interactions between the parameters.

1. Introduction

IntraOcular Pressure (IOP), as one of the most important eye-health factors, should always be measured and evaluated. Increasing this pressure can cause hypertension and glaucoma, and in severe cases, could damage the retina cells and cause blindness. The lack of this pressure changes the corneal geometry and causes malfunctions in the refraction of light and visual impairment. Therefore, its continuous monitoring is a vital task. For this purpose, several tonometers have been developed that can be divided into two main groups: (*i*) contact tonometers such as Goldman (Goldmann, 1955), Dynamic Contour Tonometer (Kaufmann et al., 2003; Kanngiesser et al., 2005) (DCT, Swiss Microtechnology AG, Port, Switzerland), and (*ii*) non-contact and non-invasive tonometers like ORA (Luce, 2005), and CorVis ST (Ambrósio et al., 2011). The commonality of all these tonometers is that they measure IOP by applying a static or dynamic mechanical load on a portion of the cornea and study the induced changes in its configuration. Therefore, the pressure measured by these tonometers is influenced by rigidity (stiffness) parameters, e.g. corneal thickness and curvature (Hsu et al., 2009; Broman et al., 2007; Kirwan and O'Keefe, 2008; Harada et al., 2008), and biomechanical properties of the cornea (Liu and Roberts, 2005). In this regard, several correctional equations and coefficients have been proposed to compensate or to reduce the effect of these factors on pressure measurement (EHLERS et al., 1975; Orssengo and Pye, 1999; Kwon et al., 2008; Chihara, 2008; Elsheikh et al., 2011).

One of the most common types of these tonometers is the non-contact CorVis tonometer. It makes deformation in the cornea by applying an air-puff and then, by using ultra-high-speed scheimpflug imaging, the Dynamic Corneal Response parameters (DCRs) and the IOP are estimated. This means that the CorVis tonometer can provide images of the corneal deformation and also a report of its dynamic parameters (Joda et al., 2015). These outputs can be used as biomarkers for eye diseases such as Glaucoma (Lee et al., 2016; Tian et al., 2016) and Keratoconus (Vinciguerra et al., 2016). However, the outcomes of this tonometer are mostly affected by the corneal hardness parameters, biomechanical properties, and pachymetry data (Ali et al., 2014). The bIOP is another

* Corresponding author. Structural Integrity & Composites, Faculty of Aerospace Engineering, Delft University of Technology, 2629 HS, Delft, Netherlands.
E-mail address: v.yaghoubi@tudelft.nl (V. Yaghoubi).

https://doi.org/10.1016/j.jmbbm.2022.105210
Received 29 August 2021; Received in revised form 17 March 2022; Accepted 26 March 2022
Available online 1 April 2022

output of the CorVis Tonometer in which the effect of the above-mentioned parameters has been taken into account (Eliasy et al., 2018). Precise knowledge of the material behavior and geometry of the cornea is thus necessary for the accurate measurement of the bIOP. However, the bIOP used previous data to generate a model and in that model, the effect of each feature has been decided by the experts' opinion (Eliasy et al., 2018). In this work, the model can be generated for each patient specifically and the contribution of each feature has been estimated mathematically. However, inappropriate numerical models could affect the DCRs (Pedersen et al., 2014; Shen et al., 2014a; Bak-Nielsen et al., 2014; Hassan et al., 2014) and, in turn, lead to erroneous pressure measurement (Hassan et al., 2014; Shen et al., 2014b). In other words, accurate measurement of the bIOP requires a proper numerical model of the cornea. And for that, two main aspects of the cornea should be considered: geometry and material model.

Studies have shown that the corneal dimensions, such as thickness and curvature, could affect the IOP measurement and change the DCR parameters (Joda et al., 2015; Huseynova et al., 2014). For instance, refractive surgery changes the thickness and curvature of the cornea which could lead to over-/under-estimation of IOP depending on the pressure calculation algorithm in tonometers. Some studies have investigated the effect of the central corneal thickness and/or radius of the corneal curvature on the CorVis estimation of IOP (CVS_IOP). However, they cannot be proper factors for the estimation of CVS_IOP due to the following reasons: (i) the differentiation between them is impossible in clinical studies, (ii) they are dependant on age, gender, and race of the patient, (iii) their distributions from the central region to the cornea edges are not the same and are different in vertical and horizontal directions (Dubbelman et al., 2006).

The challenge in material modeling of the corneal tissue is two-folded: First, which material model, e.g. viscoelastic, hyperelastic, or hyper-viscoelastic material, is to be chosen; Second, how to measure the material properties of a cornea to be used for calibration of the material model. To tackle the former, it is known that the viscosity and nonlinear elasticity vary in different corneas, depending on the type of test, the rate and type of loading, and the rate of deformation. Therefore, since the strain rate and loading rate of the CorVis test are high in this test, the cornea exhibits a hyperelastic behavior and its viscous ratio is negligible (Jannesari et al., 2018a). Moreover, some studies have considered the corneal tissue to be completely isotropic while others have modeled some corneal layers and even composite collagen fibers, and believe that the dominant mechanical behavior is dependent on the distribution of collagen fibers. But, it is well accepted that the orientation of collagen fibers and their distribution densities vary in different patients and different diseases, that is the Holzapfel material model (Bagheri et al., 2021). However, any change in the collagen orientation leads to a change in the corneal stiffness and its elastic anisotropy (Singh et al., 2016), and this, in turn, results in the IOP variation. Therefore, the mentioned complexities result in models with higher accuracy but with longer simulation time. To address the second issue, it is worth mentioning that the material properties of the cornea could be measured in in-vivo and ex-vivo methods. In this regard, some researchers have studied the corneal strips or have inflated the cornea or the eyeball. However, these tests result in the separation of corneal layers leading to changes in boundary conditions as well as the position of the layers and the collagens. Therefore, the biomechanical properties vary during the test. In determining the in-vivo properties, the measured properties are influenced by IOP, boundary conditions, corneal geometry, external loading, age, and medical history of patients.

Since, in the tonometers, the force is applied on the outer surface of the cornea, the response is a combination of motion and deflection in the eyeball. This means that the fatty tissues behind the eyes and the muscles that control the overall movement of the eye should be considered. However, they have age-dependent properties that cannot be captured by the CorVis imaging. Therefore, this tissue and its modeling could affect the images and outputs of the CorVis tonometer. To take into account the effect of the fatty tissues, they have been modeled with a simple mass-spring-damper system as described in references (Jannesari et al., 2018b; Sinha Roy et al., 2015). In (Joda et al., 2015), the whole eye has been modeled which is not cost-effective in terms of time and complexity. Moreover, the errors in corneal-scleral attachment and properties of the eyeball propagate into the pressure measurement. Although some researchers have tried to separate the eye movement from the corneal deflection (Vinciguerra et al., 2016), the eyeball itself deforms and changes the curvature of the cornea. Together with the fact that the behavior and structure of the cornea change by diseases, e.g. keratoconus, glaucoma, and diabetes (Tian et al., 2014, 2016; Ye et al., 2015; Romero-Jiménez et al., 2010), environmental conditions, and refractive surgeries (Dupps and Wilson, 2006; Frings et al., 2015), this means that the calculations of the tonometers are patient-specific. In other words, in numerical modeling, some parameters should be considered as uncertain values.

In order to model physical systems with uncertain parameters, stochastic modeling techniques can be employed. This could be achieved intrusively or non-intrusively. In intrusive approaches, the equations of a system are modified to create an explicit function between the stochastic responses and the uncertain inputs of the system. Examples of such approaches are the perturbation method (Schuëller and Pradlwarter, 2009) and intrusive Polynomial Chaos Expansion (PCE) (Ghanem and Spanos, 2003). In non-intrusive approaches, the existing deterministic model is evaluated at several points sampled from the parameter space, e.g. Kriging (Fricker et al., 2011), non-intrusive PCE (Yaghoubi et al., 2017), or combinations thereof (Schobi et al., 2015). In this study, the simplifications made in the modeling of the CorVis test procedure and the lack of proper allocation of the material properties and loading conditions in the numerical models are examples of uncertainties. To create the stochastic model, the non-intrusive PCE method has been chosen. However, the major drawback of PCE methods is the presence of a large number of unknown coefficients that could occur in problems with large parameter spaces. Sparse (Blatman and Sudret, 2008) and adaptive sparse (Blatman and Sudret, 2011) polynomial chaos expansions have been developed to tackle this issue.

To the best of the authors' knowledge, there is no study available in the literature to investigate the effect of uncertainty in the inputs, i.e. the mechanical properties of the cornea, central corneal thickness and curvature, IOP, and corneal boundary conditions, on the outputs, i.e. IOP and DCR parameters. Therefore, the major contribution of this study is to develop a stochastic model based on adaptive-sparse PCE for efficient and accurate prediction of the internal pressure of the cornea. In this regard, the main novelties of the current study are:

1 Developing a deterministic finite element model of the cornea to properly simulate the CorVis tonometry process, and to obtain IOP and DCR parameters for one specific case.
2 Proposing a new two-stage surrogate modeling technique based on adaptive sparse polynomial chaos expansion (PCE) to efficiently and accurately predict IOP and DCR parameters for each patient
3 Performing sensitivity analysis by using PCE-based Sobol indices to quantify the effect of each input on the outputs.

2. Materials and methods

Nonlinear finite element analysis of the CorVis tonometer process for corneas with specific and controllable geometry, biomechanical properties, internal pressure, and boundary conditions were carried out using ABAQUS finite element software (6.14). Python as the built-in programming language of the ABAQUS was used for parameterizing the FE model. Then, by using the UQLAB plugin (Marelli and Sudret, 2014) from MATLAB software, the finite element model was transformed into a stochastic model. At last, the sensitivity analysis was performed.

3. Deterministic modeling

3.1. Geometry

The Corneal thickness and curvature vary from central region to limbus area. According to studies, the corneal thickness is generally lower in the center and is thicker in the edges. Therefore, in a primary geometry, the inner curvature of the cornea is supposed to be larger than its outer curvature (Dubbelman et al., 2006) so that the corneal thickness increases from the center to edge. On the other hand, since the study of the effect of thickness and curvature on different quantities is considered, corneal geometry and its properties are modeled axisymmetric, as shown in Fig. 1a. CorVis tonometer device also calculates its parameters based on a cross-sectional area of the cornea, which is located along the horizontal meridian of the cornea. The local curvature varies in different directions of each cornea, and the distribution of corneal thickness and curvature vary due to diseases. Therefore, since clinical studies and mechanical models rely on central corneal thickness and curvature, these results are only qualitatively acceptable. While in this study the corneal curvature is the same in all regions, the thickness of each region is also a function of the central corneal thickness. In order to reduce the errors due to extraocular muscles and fatty tissue behind the eye, the cornea is fully bounded to eliminate the effects of boundary conditions so only corneal deformation is reported as shown in Fig. 1b.

3.2. Loading

The simulation of the CorVis tonometry test is performed in two steps in ABAQUS software. First, in a static step, internal pressure (IP) is applied to the inner surface of the cornea, which causes the initial geometry of the cornea to be altered under the pressure of the aqueous humor. This should be emphasized that, in contrast to the IOP which is a clinical parameter to be measured, the IP is a modeling parameter that should be set. In the second step, the spatial and temporal distribution of the air pressure is applied to the outer surface of the cornea at a time interval of 32 ms in a dynamic step (Dynamic, Implicit) with the use of the subroutine DLOAD, which receives all the dynamic responses at that time.

3.3. Corneal behavior and structure

Most of the previous studies have considered corneal behavior as a linear elastic material (Asejczyk-Widlicka et al., 2004; Schutte et al., 2006; Rangarajan et al., 2009). By examining laboratory and clinical topographies, it was concluded that the cornea also has viscoelastic behavior. The progressive deformation of the cornea in the keratoconus (Shah et al., 2007) and the changes made after the common refractive surgeries (Kerautret et al., 2008) are probably due to a change in the time-dependent stress distribution in the cornea, i.e. due to its viscoelastic deformation. In addition, in some studies, corneal behavior has been modeled as hyperelastic (Han et al., 2013; Nguyen and Boyce, 2011; Bekesi et al., 2016). But, nowadays, it can be deduced that the human cornea has both hyperelastic and viscoelastic properties (Cui et al., 2015; Whitford et al., 2017). However, due to the high loading rate and applied strains in the CorVis test, it can be concluded that the cornea exhibits hyperelastic behavior in this test so its viscosity is negligible (Jannesari et al., 2018a, 2018b). In this regard, the theory of isotropic non-linear elastic material is considered. In this theory, the strain energy per unit of reference volume W depends on the two coefficients C_{10} and D_1 as the material constants of the model that should be measured for each cornea. It is

$$W = C_{10}(\bar{I}_1 - 3) + \frac{1}{D_1}(J-1)^2 \tag{1}$$

where $\bar{I}_1$ is the first invariant of the left Cauchy-Green deformation tensor, and J is the elastic volume ratio.

3.4. Reconstruction of the CorVis tonometer parameters

Since there is no direct access to the anterior chamber of the eye and its fluid, and corneal tissue's property is unknown, the CorVis tonometer is used in a loading process as an intermediate device to measure intermediate parameters called dynamic corneal parameters. Afterward, this tonometer analyzes the intermediate parameters to identify the biomechanical properties of the cornea and eye tissue. The first applanation time (t_{A_1}), the deflection amplitude (Def), the highest deflection amplitude (Def_H), the applanation length (L_{A_1}), and the peak distance (PD) are the most important dynamic parameters, see Fig. 2, reported by the CorVis tonometer, which are effective in IOP measurement and corneal tissue identification. However, the effectiveness of these parameters has been reported neither qualitatively nor quantitatively. Therefore, the first applanation time for each simulation was calculated using Python software; then, the other related parameters were computed including applanation length and deflection amplitude. The highest corneal deflection was also detected by the Python code and the peak distance is calculated. In addition, given that the corneal surface is discretized in simulations, the number of increments should be high enough so that the criteria for recognizing dynamic parameters could understand the smallest changes made in the dynamic parameters for changes in the initial factors.

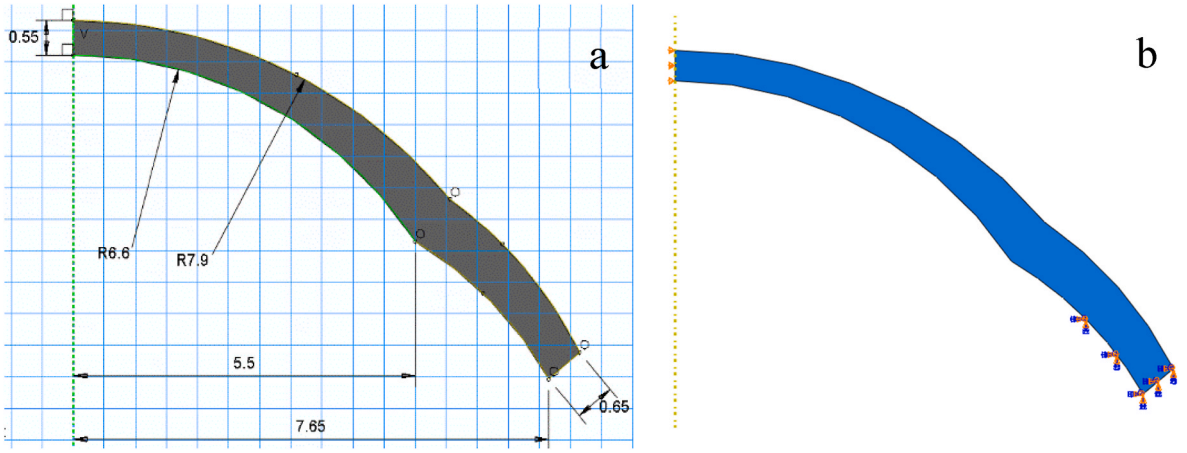

Fig. 1. a. Basic geometry of human cornea for FEA (in millimeters) b. Boundary conditions of a human cornea.

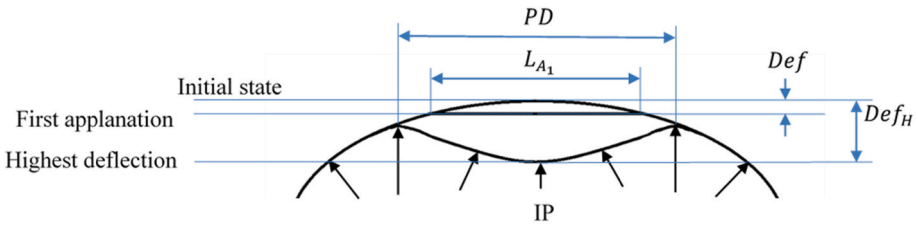

Fig. 2. Schematic of the cornea at three states: initial, first applanation, and the highest deflection. The associated parameters are also shown.

4. Stochastic modeling

4.1. Mathematical background

Surrogate models are mathematical functions that replace the computationally expensive models and, without any knowledge about the physics of the problem at hand, could approximate a response with high precision in much less simulation time. Polynomial Chaos Expansions (PCE) is a powerful surrogate modeling technique that is employed here. In this section, some topics pertinent to PCE are first briefly introduced; then, the sensitivity analysis by using the PCE-based surrogate model is presented.

4.1.1. PCE-based surrogate model

First, assume that the computational model of a physical system is in the form $\mathscr{M}: \boldsymbol{X} \rightarrow \boldsymbol{Y} = \mathscr{M}(\boldsymbol{X})$. Here $\boldsymbol{X} = \{X_1, \ldots, X_M\}$ and $\boldsymbol{Y}$ are the random inputs and output of the model. Also, assume that random variables $\boldsymbol{X}$ are independent with joint probability density function of $f_{\boldsymbol{X}}(\boldsymbol{x}) = \prod_{i=1}^{M} f_{X_i}(x_i)$. Then, the polynomial chaos expansion of the model $\mathscr{M}$ is defined as:

$$\boldsymbol{Y} = \mathscr{M}(\boldsymbol{X}) = \sum_{\boldsymbol{\alpha} \in \mathbb{N}^M} \lambda_{\boldsymbol{\alpha}} \Psi_{\boldsymbol{\alpha}}(\boldsymbol{X}) \tag{2}$$

where the $\Psi_{\boldsymbol{\alpha}}(\boldsymbol{X})$ are multi-variable polynomials orthonormal chosen with respect to the distribution of inputs, $\boldsymbol{\alpha} \in \mathbb{N}^M$ is a multi-index ($\boldsymbol{\alpha} = (\alpha_1, \ldots, \alpha_M)$) indicate the polynomial degree of the components of $\Psi_{\boldsymbol{\alpha}}$, and $\lambda_{\boldsymbol{\alpha}}$ denotes its associated coefficients which should be estimated. In realistic applications, Eq. (2) is converted into a finite summation, i.e., the truncated polynomial chaos expansion:

$$\mathscr{M}(\boldsymbol{X}) \approx \mathscr{M}^{PCE}(\boldsymbol{X}) = \sum_{\boldsymbol{\alpha} \in A} \lambda_{\boldsymbol{\alpha}} \Psi_{\boldsymbol{\alpha}}(\boldsymbol{X}) + \varepsilon_t \equiv \boldsymbol{\Lambda}^T \Psi(\mathbf{X}) + \boldsymbol{\varepsilon} \tag{3}$$

in which $(\cdot)^{PCE}$ stands for the polynomial chaos expansion, $A \subset \mathbb{N}^M$ with cardinality P is the set of multi-indices selected based on the truncation scheme, and ε_t is the truncation error. To estimate the coefficients $\lambda_{\boldsymbol{\alpha}}$ by non-intrusive techniques, one should minimize ε_t. To this end, let $\mathcal{X} = \{\boldsymbol{x}^{(1)}, \boldsymbol{x}^{(2)}, \ldots, \boldsymbol{x}^{(N_{ED})}\}$ be an experimental design with N_{ED} space-filling samples of $\boldsymbol{X}$ and $\mathcal{Y} = \{\boldsymbol{y}^{(1)} = \mathscr{M}(\boldsymbol{x}^{(1)}), \boldsymbol{y}^{(2)} = \mathscr{M}(\boldsymbol{x}^{(2)}), \ldots, \boldsymbol{y}^{(N_{ED})} = \mathscr{M}(\boldsymbol{x}^{(N_{ED})})\}$ be their associated responses. Then, the minimization problem is

$$\widehat{\boldsymbol{\Lambda}} = \operatorname{argmin} \mathbb{E}\left[\left(\boldsymbol{\Lambda}^T \boldsymbol{\Psi}(\boldsymbol{X}) - \mathscr{M}(\boldsymbol{X})\right)^2\right] \tag{4}$$

with the closed-form solution as

$$\widehat{\boldsymbol{\Lambda}} = \left(\boldsymbol{\Psi}^{\mathrm{T}} \boldsymbol{\Psi}\right)^{-1} \boldsymbol{\Psi}^{\mathrm{T}} \mathcal{Y} \tag{5}$$

here $\boldsymbol{\Psi}$ is a matrix with elements $\boldsymbol{\Psi}_{ij} = \psi_{\alpha_j}(\boldsymbol{x}^{(i)})$, $i = 1, 2, \ldots, N_{ED}$, $j = 1, 2, \ldots, P$.

To avoid overfitting, the least square problem can be solved by using adaptive sparse regression algorithms such as the Least Angle Regression (LAR) algorithm (Blatman and Sudret, 2011). The accuracy of the representation is estimated by means of the leave-one-out (LOO) cross-validation as presented in (Blatman and Sudret, 2008). Given the sample set $\boldsymbol{\chi} = \{\boldsymbol{x}^{(1)}, \boldsymbol{x}^{(2)}, \ldots, \boldsymbol{x}^{(n)}\}$ and the system output $\mathcal{Y} = \{\boldsymbol{y}^{(1)}, \boldsymbol{y}^{(2)}, \ldots, \boldsymbol{y}^{(n)}\}$, the LOO error is defined as:

$$\varepsilon_{LOO} = \frac{1}{n} \sum_{i=1}^{n} \left(\frac{y^{(i)} - \mathscr{M}^{PCE}\left(x^{(i)}\right)}{1 - h_i} \right)^2 \tag{6}$$

where h_i is the i^{th} diagonal term of the matrix $\boldsymbol{\Psi}(\boldsymbol{\Psi}^{\mathrm{T}}\boldsymbol{\Psi})^{-1}\boldsymbol{\Psi}^{\mathrm{T}}$ as defined in Eq. (15). In practice, a normalized version of the Err_{LOO} is used:

$$\varepsilon_{LOO} = \frac{\varepsilon_{LOO}}{Var(\mathscr{Y})} \tag{7}$$

where Var($\mathscr{Y}$) is the sample variance of the system response.

4.1.2. PCE-based sensitivity analysis

Sensitivity analysis should be performed to quantify the importance of the random inputs to the outputs. This could be beneficial in better understanding of the model, prioritizing the input parameters, possibly removing some of them, and thus simplifying the model. For this purpose, Sobol indices is one of the established methods (Sobol, 1993). It is based on the idea of expanding the output variance into the summands of variances in the input parameters. That is,

$$\operatorname{Var}(Y) = \sum_{i=1}^{M} V_i + \sum_{1 \le i < j \le M} V_{ij} + \ldots + V_{12\ldots M} \tag{8}$$

in which V_i is the effect of parameter X_i on the output Y. V_{ij} is the joint effect of interactive term X_i and X_j and $V_{12\ldots M}$ is the interaction of all M parameters on the output Y. Then the Sobol sensitivity indices are,

$$S_i = \frac{V_i}{Var(Y)} i = 1, 2, \ldots., M \tag{9}$$

as the first order,

$$S_{ij} = \frac{V_{ij}}{Var(Y)} i, j = 1, 2, \ldots., M, j \neq i \tag{10}$$

as the second order sobol indices. The total effect is,

$$S_i^T = S_i + \sum_{\substack{j=1 \\ j \neq i}}^{M} S_{ij} + \ldots + S_{12\ldots M} \tag{11}$$

Given a PCE-based surrogate model, these indices can be calculated for free (Sudret, 2008). For this purpose, Eq. (3) can be rewritten as:

$$\mathscr{M}(\boldsymbol{X}) \approx \mathscr{M}^{PCE}(\boldsymbol{X}) = \sum_{\boldsymbol{\alpha} \in A} \lambda_{\boldsymbol{\alpha}} \Psi_{\boldsymbol{\alpha}}(\boldsymbol{X}) = \lambda_0 + \sum_{\substack{u \subset \{1, \ldots, M\} \\ u \neq \emptyset}} \sum_{\boldsymbol{\alpha} \in A_u} \lambda_{\alpha} \Psi_{\boldsymbol{\alpha}}(\boldsymbol{X}) \tag{12}$$

in which, for any non-empty set $\boldsymbol{u} \subset \{1, \ldots, M\}$, $\mathscr{A}_u$ contains all multi indices $\boldsymbol{\alpha} \in \mathscr{A}$ which have non-zero components $\alpha_k \neq 0$ if and only if $k \in \boldsymbol{u}$. Then, the Sobol indices can be obtained as,

$$S_u = \frac{Var(Y_u(\boldsymbol{x}_u))}{Var(Y(\boldsymbol{x}))} = \left[\sum_{\substack{\alpha \in \mathscr{A}_u \\ \alpha \neq 0}} \lambda_{\alpha}^2 \Big/ \sum_{\substack{\alpha \in \mathscr{A} \\ \alpha \neq 0}} \lambda_{\alpha}^2 \right] \tag{13}$$

4.2. The proposed methodology

In this section, different steps of the proposed method are explained. Fig. 3 shows the building blocks of the procedure consisting of two main stages:

I) FEM-driven PCE-based surrogate model: at this step, a PCE model is created to replace the FE model generated in Section 1. This is elaborated in Section 2-2-1.
II) Data-driven PCE-based surrogate model: at this step, the PCE is used to make a model to estimate the pressure (IP). This is explained in Section 2-2-2.

These steps are implemented in MatLab by using the UQLAB toolbox (Marelli and Sudret, 2014).

4.2.1. FEM-driven PCE-based surrogate model (PCE_{FD})

Predicting the intermediate parameters of the CorVis tonometer by the FE model, see Section 1, is a computationally expensive task. Therefore, the target of this stage is to replace it with a surrogate model. For this purpose, the following steps should be taken:

1 Choosing inputs of the FE model: The input vector has been chosen to be the following 5-dimensional vector,

$$\text{Input space I}: X_I = \{CCT, IP, \rho, C_{10}, D_1\} \subset \mathbb{R}^5 \tag{14}$$

in which, CCT is the central corneal thickness, IP is the applied internal pressure, ρ is the radius of external curvature, and C_{10} and D_1 are the constants of the Neo-Hookean hyperelastic material model.

2 Creating a parameter space from the clinical dataset: A large population of clinical data is used to provide inclusive parameter space for the input parameters. Since the properties and geometries of healthy eyes vary in different parts of the world, information on healthy eyes and corneas was extracted from several sources (Joda et al., 2015; Lee et al., 2016; Jannesari et al., 2018a, 2018b; Shah et al., 2007; Lopes et al., 2017; Smedowski et al., 2014; Nemeth et al., 2017; Kohlhaas et al., 2006). A Gaussian distribution has been assumed for each parameter. They are illustrated in Fig. 3.

3 Generating the experimental design: This has been carried out by using the Sobol sampling method. It should be mentioned that some of the samples may not be compatible with the physical facts and mathematical principles. Such samples have been thus deleted.

4 Evaluating the FE model at the samples: the selected sample points have been transmitted to the Python code. The FE model was evaluated and the outputs of interest were received. Here, the outputs of interest are the intermediate CorVis parameters, i.e.

$$\text{Output space I}: Y_I = \{Def, Def_H, t_{A_1}, L_{A_1}, PD\} \subset \mathbb{R}^5 \tag{15}$$

5 Making the PCE-based surrogate model $\mathscr{M}_{FD}^{PCE}$: since the input parameters have been assumed to be Gaussian, the Hermite polynomial should be selected as the basis. One PCE model has been made for each output, their coefficients were estimated by the LARS approach with a maximum polynomial degree of 10.

Having this PCE model, one could simply propagate the uncertainty in the input parameters through the model to estimate the uncertainty in the output parameters, i.e. intermediate CorVis parameters. This is called uncertainty propagation. Further, the PCE model could be used to perform the sensitivity analysis to highlight the important input parameters.

4.2.2. Data-driven PCE-based surrogate model (PCE_{DD})

At this stage, a surrogate model is generated to predict the pressure applied to the inner surface of the cornea (IP). In this regard, to create the input space, the intermediate CorVis parameters obtained in the previous section have been employed. Since this procedure is the inverse

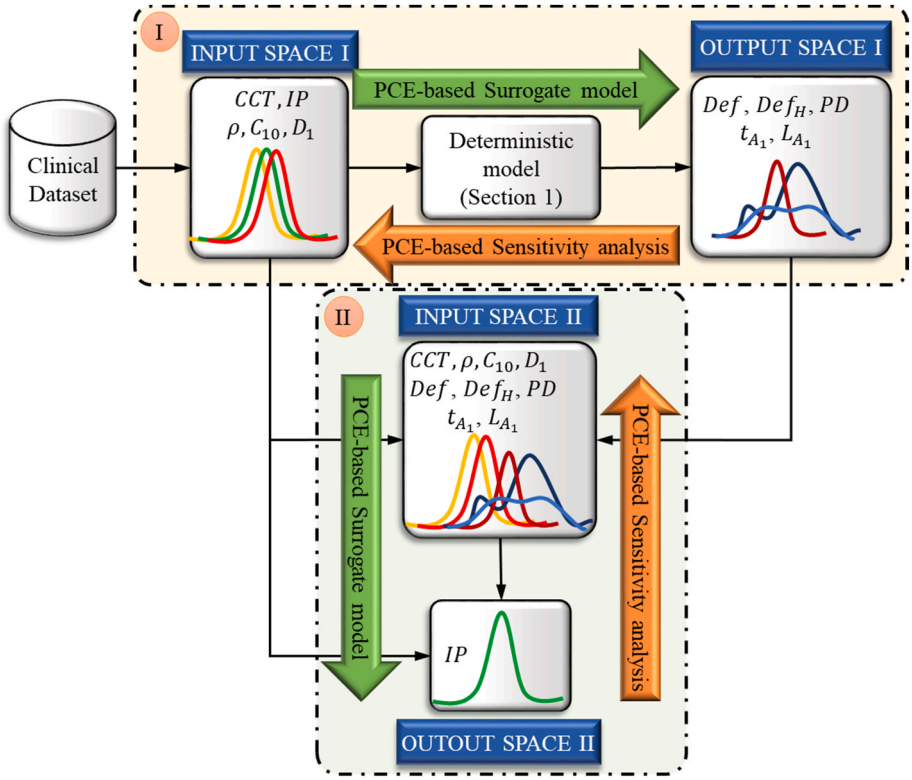

Fig. 3. The used process to build the internal pressure surrogate model.

of the PCE model built in the previous section, one could consider it as an estimation of the inverse PCE model by another PCE. However, to take into account the effect of geometries and material properties of the cornea on the IP, they are included in the input space. This is in accordance with the well-known issue that the IP estimated by the CorVis parameters needs to be corrected (Joda et al., 2015). Therefore, the input and output spaces of this PCE model are,

$$\text{Input space II}: X_{II} = X_I \backslash \{IP\} \cup Y_I = \{CLT, \rho, C_{10}, D_1, Def, Def_H, t_{A_1}, L_{A_1}, PD\} \subset \mathbb{R}^9 \tag{16}$$

$$\text{Output space II}: Y_{II} = \{IP\} \tag{17}$$

The main challenge here is to create the required experimental design for making the PCE. Since the parameters in Y_I are functions of X_I, sampling the input space II can not be performed randomly. Moreover, since no explicit function for predicting the IP is available, obtaining true IP for each input parameter set is another issue. In this regard, the following procedure is proposed:

1 Sampling the input space I, $\mathscr{X}_I \in X_I$,
2 Evaluating the FEM-driven PCE model, $\mathscr{Y}_I = \mathscr{M}_{FD}^{PCE}(\mathscr{X}_I)$.
3 Creating the experimental design for the data-driven PCE as $\mathfrak{E} = \{\mathscr{X}_I \backslash \{IP\} \cup \mathscr{Y}_I\}$ and their associated output as $\mathscr{Y}_{II} = IP$.

Then, the data-driven PCE model $\mathscr{M}_{DD}^{PCE}$ could be built over the experimental design $\mathfrak{E}$ and output IP.

5. Results and discussion

Fig. 4 shows deformations obtained by the FE model of a cornea with random properties before and after applying the air-puff. The whitened part of the figure is a copy of the main result. It has been added just for illustration purposes. This result shows high qualitative correlation between the FE model's output and the experimental data shown in Fig. 5 (Bekesi et al., 2016).

A Gaussian distribution has been fitted to each stochastic input parameter of the FE model. Fig. 6 shows these distributions. To make the FE-driven PCE surrogate model, the Hermite polynomial has been selected as the basis. 400 points have been sampled from the parameter space to generate the experimental design. The FE model was evaluated at these points.

LARS algorithm has been employed to make sparse PCEs with adaptive degrees up to order 10. For further reduction in the number of unknown coefficients of the PCEs, a hyperbolic truncation with a q-norm of 0.7 was utilized prior to LARS algorithm. Moreover, only polynomials up to rank 2 were selected here (i.e. polynomials that depend at most on 2 parameters). A convergence analysis has been performed by evaluating the LOO error by enlarging the experimental design. The results presented in Fig. 7 illustrate the accuracy of the built PCEs for all the outputs except for the first applanation length L_{A_1}. In the convergence analysis of the surrogate model of the L_{A_1}, it can be seen that, although its error was reduced, the rate of its error reduction was so low and, even after 400 cases, it still has 30% error. Therefore, we stop using this output parameter for further investigation.

Now, to choose the polynomial bases of the PCE_{DD} model, one should first estimate the distribution of the PCE_{FD} model's output. For this purpose, 100,000 samples have been extracted from the parameter space to feed the PCE_{FD} model. It took 0.2 s for the surrogate model to deliver the whole results but for FEM, each simulation took around 1 h. The result has been shown in Fig. 8 in the form of histograms. A normal distribution has been assigned to the distribution of the deflection whereas, a lognormal distribution has been fitted to the other outputs. Therefore, the Hermite polynomials have been chosen as the bases of the PCE_{DD}. It is worth mentioning that, for lognormal distributions, the Hermite polynomials on the transformed variable $\boldsymbol{Z} = \ln(\boldsymbol{X})$ has been used to make the polynomial bases as follows,

$$Y = \mathscr{M}^{PCE}(\boldsymbol{X}) = \sum_{\boldsymbol{\alpha} \epsilon A} \lambda_{\boldsymbol{\alpha}} \Psi_{\boldsymbol{\alpha}}(\ln(\boldsymbol{X})) \tag{18}$$

The next step is to create an experimental design. For this purpose, first, 10,000 points sample from the "input space I″ and send it to the PCE_{FD} to predict their outputs. The combination of the outputs with the input parameters except for the IP made the required ED. The IP has been used as the output. Then, the LARS algorithm has been used to build a sparse PCE_{DD} model with the adaptive degree. Here, a q-norm of 0.7 has been chosen. The obtained model has the LOO cross-validation error of 0.39%, indicating the model is highly accurate. However, to display this accuracy on a separate validation dataset, 10,000 new samples have been extracted from the "Input space I″ and passed through the proposed procedure to predict IP. The result is presented in the left plot in Fig. 9. Comparing this figure with its corresponding one obtained from the clinical data, IOP in Fig. 6, reveals the accuracy of the proposed procedure in predicting the distribution of the IP. Moreover, the accuracy of the proposed procedure in predicting one IP is illustrated

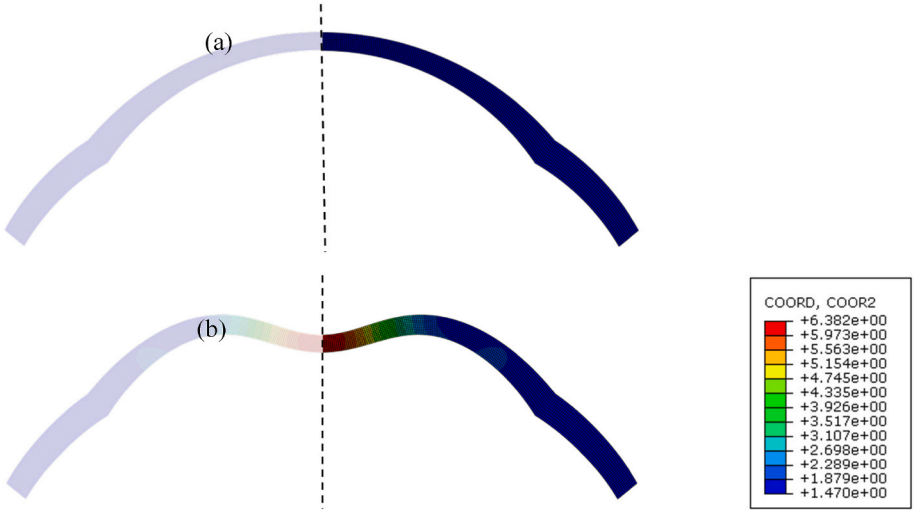

Fig. 4. Deformation of the FE model of the cornea, a) before applying the air-puff, b) after applying the air-puff, at the highest concavity. The whitened part is a copy of the main results. The colors indicate the deformation due to the air-puff. (For interpretation of the references to color in this figure legend, the reader is referred to the Web version of this article.)

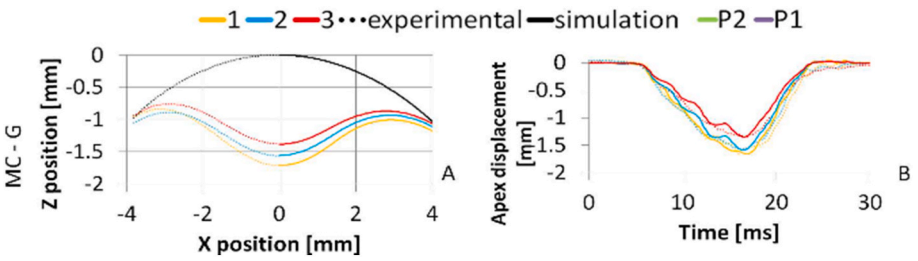

Fig. 5. Spatial and temporal deformation profiles of model cornea for qualitative comparison (Bekesi et al., 2016).

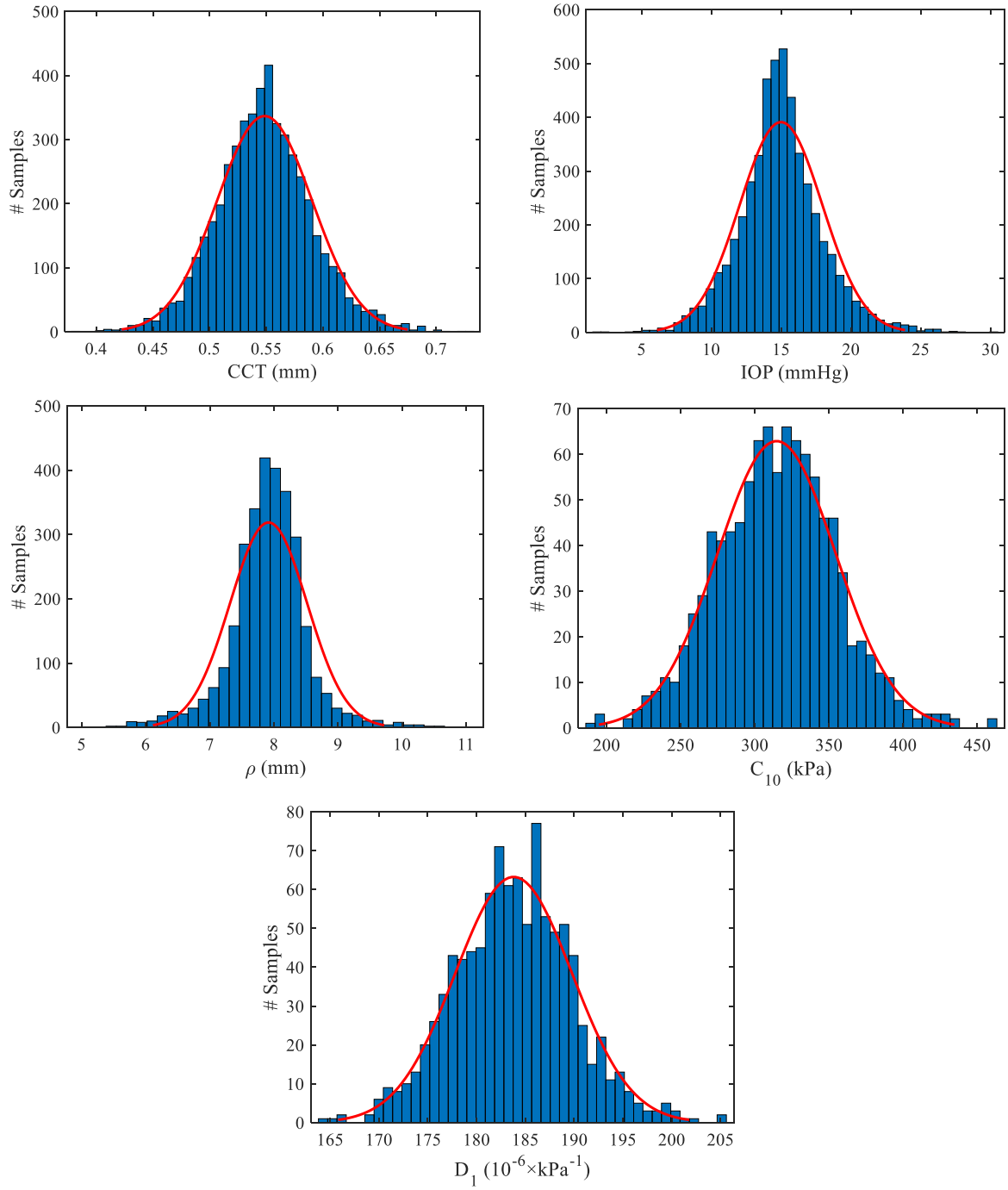

Fig. 6. Marginal distributions of the parameters in the input space I, estimated from the clinical data.

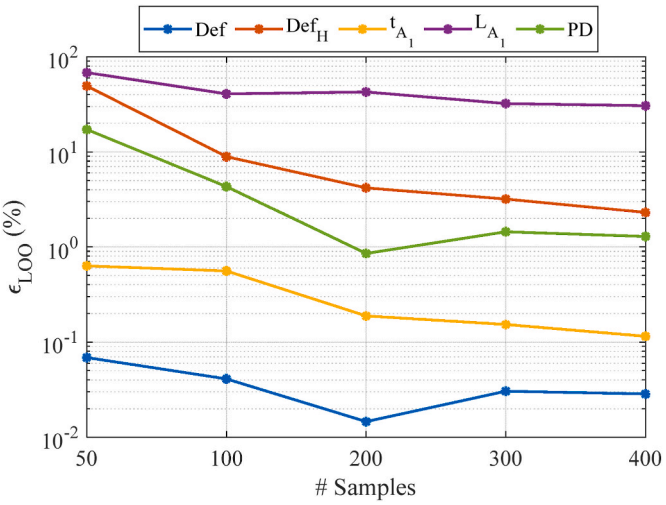

Fig. 7. Leave-one-out cross-validation error for the FEM-driven PCE model $\mathscr{M}_{FD}^{PCE}$.

by its comparison with its corresponding true one extracted from the "Input space I″, i.e. IP^{true} by the following error equation,

$$Relative\ error = \frac{\left|IP^{true} - IP^{PCE}\right|}{IP^{true}} \times 100 \tag{19}$$

here, IP^{PCE} is the internal pressure predicted by the PCE models. The outcome, shown in Fig. 9, indicates the high accuracy of the whole procedure. For further analysis of the model's performance, the IP range has been divided into 4 regions at each of which, the lative errors have been assessed and depicted in Fig. 10. This indicates the high accuracy of the model in different regions.

It should be emphasized that the sampling procedure may lead to some samples against the physics and mathematics of the problem, e.g. samples with deflection larger than the maximum deflection. Although such samples occur very rarely and, thus, cannot affect the accuracy of the models, in the current work, we have removed them from the experimental design.

One of the main issues of measuring IOP by tonometer is its high dependence on the eye geometry. This could lead to erroneous pressure reports, for instance, before and after eye refractive surgery in which the corneal curvature and thickness are changed but the IOP should remain constant (Hsu et al., 2009; Lee et al., 2017). To investigate this effect, two cases have been considered with the same internal pressure but with different thicknesses and curvatures to resemble before and after surgery, (see Table 1). As a result, the pressures measured by the innovative method of this study are calculated with high precision.

5.1. Sensitivity analysis and parameter study

Fig. 11 shows the sensitivity analysis of the output parameters. In the figures, diagonal and off-diagonal elements respectively indicate the first- and second-order indices. Total Sobol indices are shown by "Total" in the abscissa.

As can be seen, CCT, ρ, and C_{10} are the most influential parameters on the outputs whereas D_1 has almost no effect. The interaction between ρ and CCT is the biggest second-order index. The effect of other interaction terms is negligible. Moreover, the following statement can be inferred,

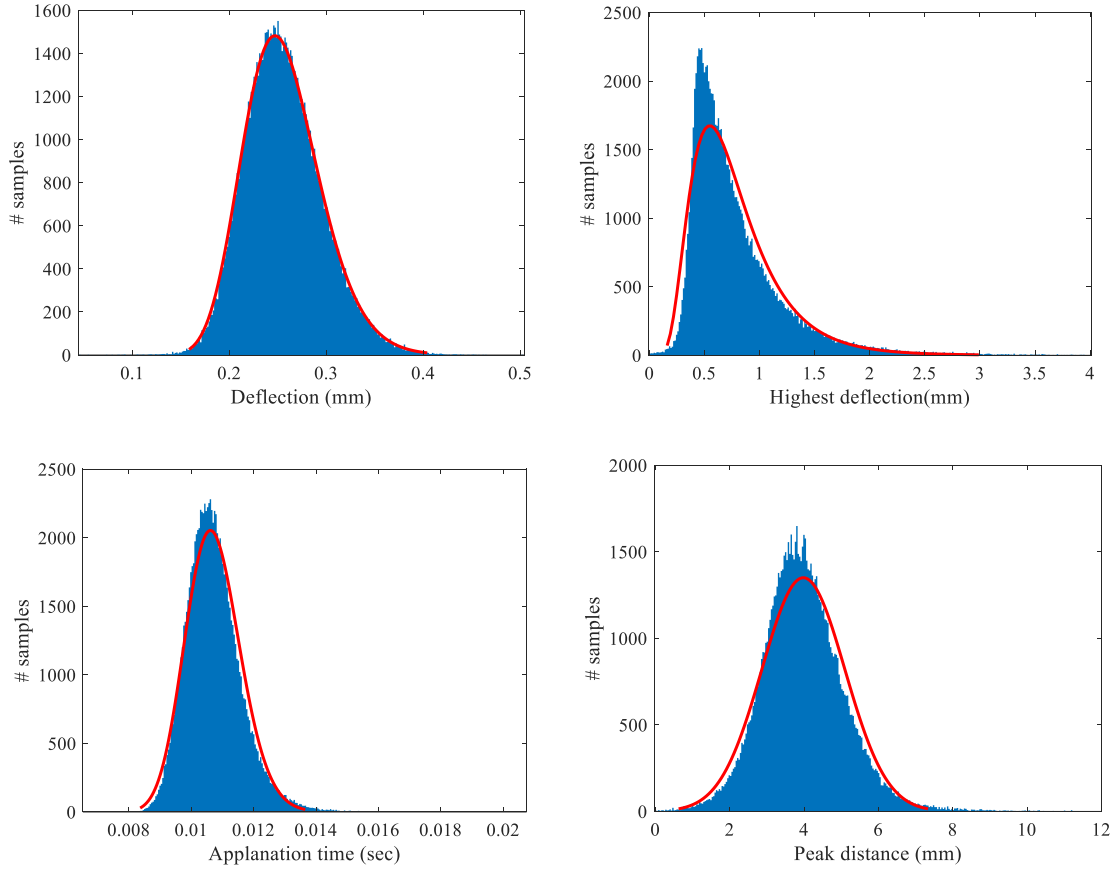

Fig. 8. Distribution of the outputs of FE-driven PCE model.

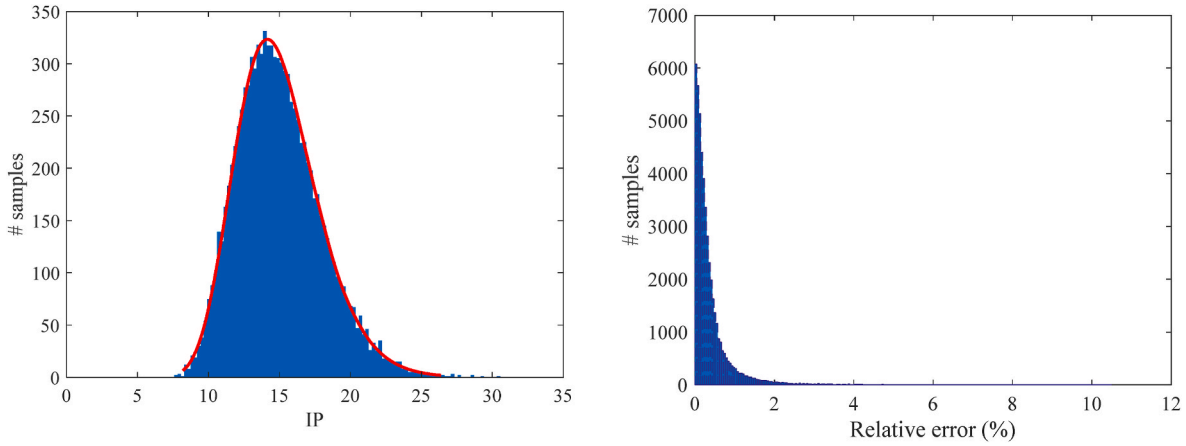

Fig. 9. Left) distribution of the internal pressure estimated by using the proposed procedure. Right) distribution of the relative error between the estimated IP and the true IP.

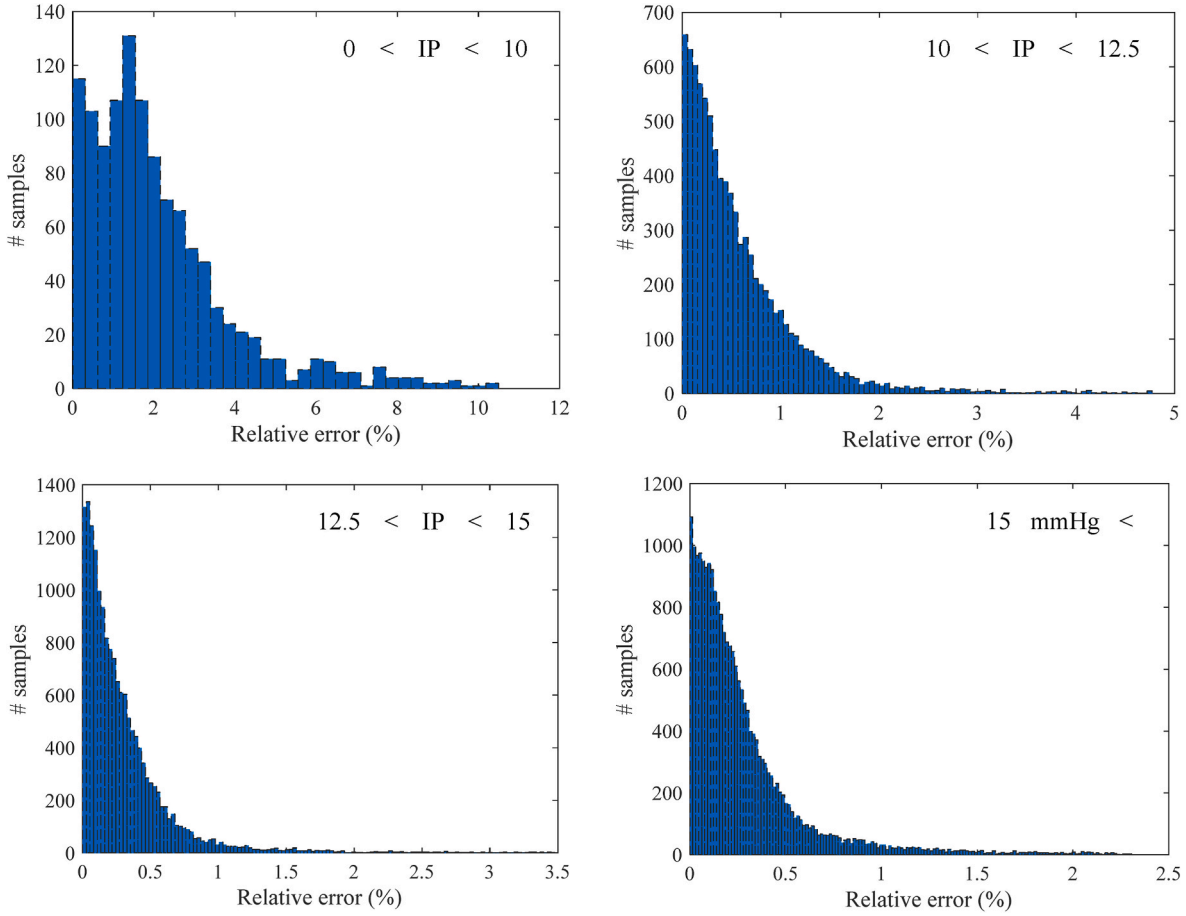

Fig. 10. Relative error calculated in four region of the internal pressure (IP).

i The Deflection amplitude can be estimated in all corneas, regardless of material properties, i.e. C_10 and D_1. It implies that the deflection can be a proper indicator for some eye diseases such as keratoconus since the radius of curvature and corneal thickness change in this disease.

ii In the highest deflection, the interaction of ρ and CCT makes a big impact. Besides, the material model C_{10} plays an important role.

iii First applanation time is one of the important outputs for the estimation of the biomechanical properties of the cornea because it is very sensitive to the C_{10}.

iv Peak distance shows a similar sensitivity pattern to the highest deflection because it is related to the time of the highest deflection. However, here, ρ is less influential whereas C_{10} become more important parameters.

The Sobol indices give the score of importance to each input parameter, but it does not provide any information about the direction of the sensitivity. Therefore, a complementary analysis would be a parameter study. In the following, this analysis has been made by using the FE model around the reference point: $CCT = 0.5\ mm$, $IP = 15\ mmHg$,

Table 1
Effect of variation in geometry on the IP, resembling before and after eye surgery.

No.	Properties	PCE_{FD}	PCE_{DD}	Relative error (%)
1	$CCT = 0.55$ mm $IP = 15.00$ mmHg $\rho = 7.9$ mm $C_{10} = 0.316$ MPa $D_1 = 0.184$ MPa^{-1}	$Def = 0.2536$ mm $t_{A1} = 0.0107$ s $Def_H = 0.6362$ mm $PD = 3.8178$ mm	$Y_{IP} = 14.8526$ $mmHg$	0.98
2	$CCT = 0.51$ mm $IP = 15.00$ mmHg $\rho = 7.95$ mm $C_{10} = 0.316$ MPa $D_1 = 0.184$ MPa^{-1}	$Def = 0.2355$ mm $t_{A1} = 0.0101$ s $Def_H = 0.8591$ mm $PD = 4.4997$ mm	$Y_{IP} = 15.1068$ $mmHg$	0.71

$\rho = 7.8\ mm,\ C_{10} = 0.316\ MPa, D_1 = 0.185\ MPa^{-1}$. In order to show the effect of different parameters in one plot, the parameters have been normalized to be in the range [0, 1]. The results are shown in Fig. 12. They also confirm the importance of the ρ, CCT, and C_{10}. However, as can be observed that all the outputs are inversely proportional to the ρ except for the first applanation length in which the relation seems nonlinear. Deflection amplitude and first applanation time are directly proportional to the CCT and C_{10} whereas the highest deflection and peak distance are inversely proportional to them. Moreover, except for the first applanation time, the other outputs are directly proportional to the Internal pressure. The figures also confirm the negligible effect of D_1. The first applanation length shows high sensitivity with direct proportionality to CCT but with negligible sensitivity to the other parameters.

5.2. Sensitivity analysis of the internal pressure

To obtain the most effective parameters for the internal pressure, a sensitivity analysis has been performed. The result is shown in Fig. 13. In this figure, the Cyan bars show the first-order Sobol indices whereas, the red bars stand for the total Sobol indices. Since most of the red bars have been hidden behind the first-order Sobol indices, the visible red parts show the effect of higher-order Sobol indices which is negligible. As can be seen in this figure, the applied internal pressure is significantly sensitive to Def, ρ, t_{A_1}, and mildly to C_{10}. Its sensitivity to other factors is negligible. This implies that one can remove the CCT, D_1, Def_H, PD, and cautiously C_{10} from the input space and reduce its dimension to three. This means that, for each new patient, it is enough to measure the radius of curvature using the Pentacam device. Then, by positioning the cornea against an air-jet to estimate first applanation time and deflection amplitude, one could estimate the internal pressure with high accuracy by using the model presented in this study.

6. Conclusion

This paper presents a probabilistic model to calculate IOP using finite element simulation responses from the CorVis tonometer test. The

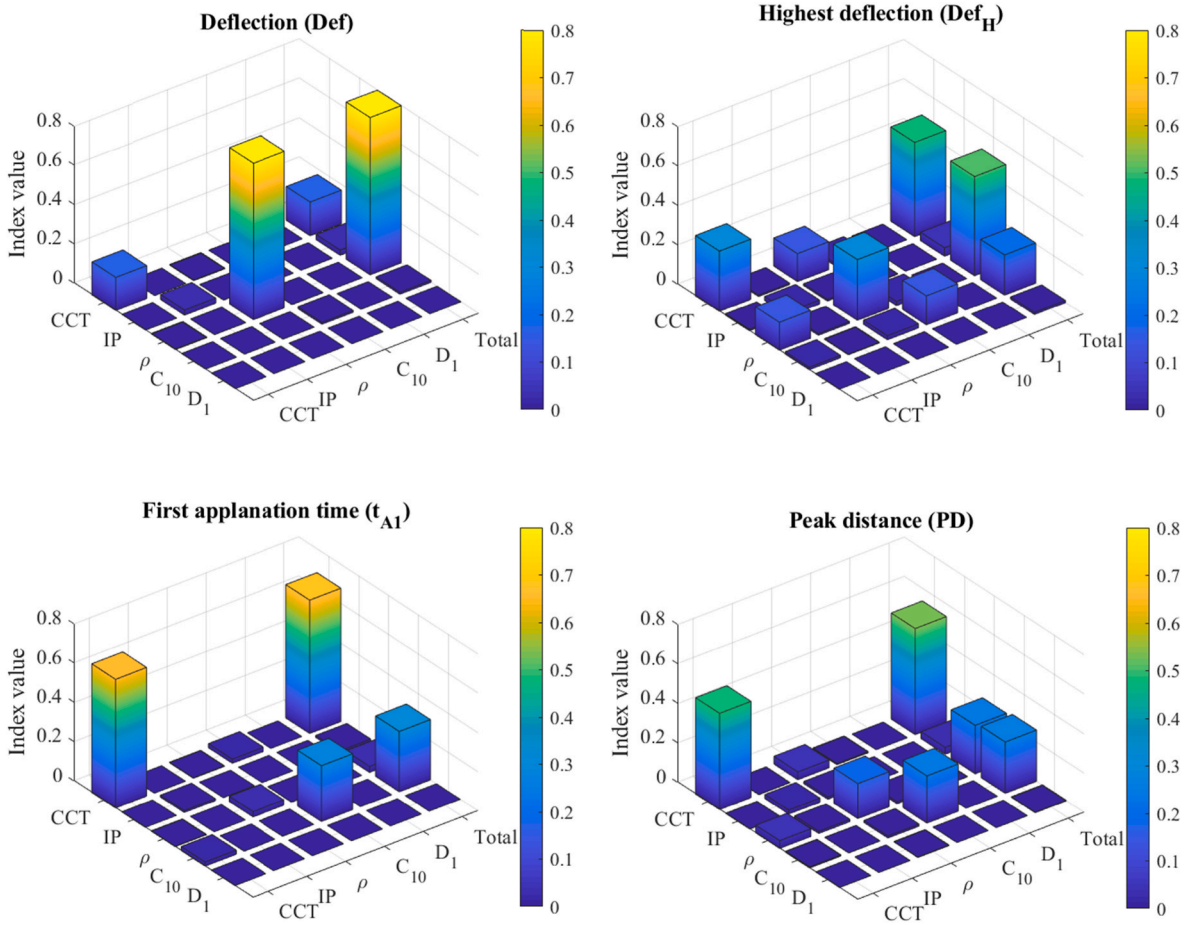

Fig. 11. Sensitivity analysis of the outputs of the FE model based on the Sobol indices. Diagonal and off-diagonal bars respectively indicate the first and second-order Sobol indices. Total indices are shown in the last column.

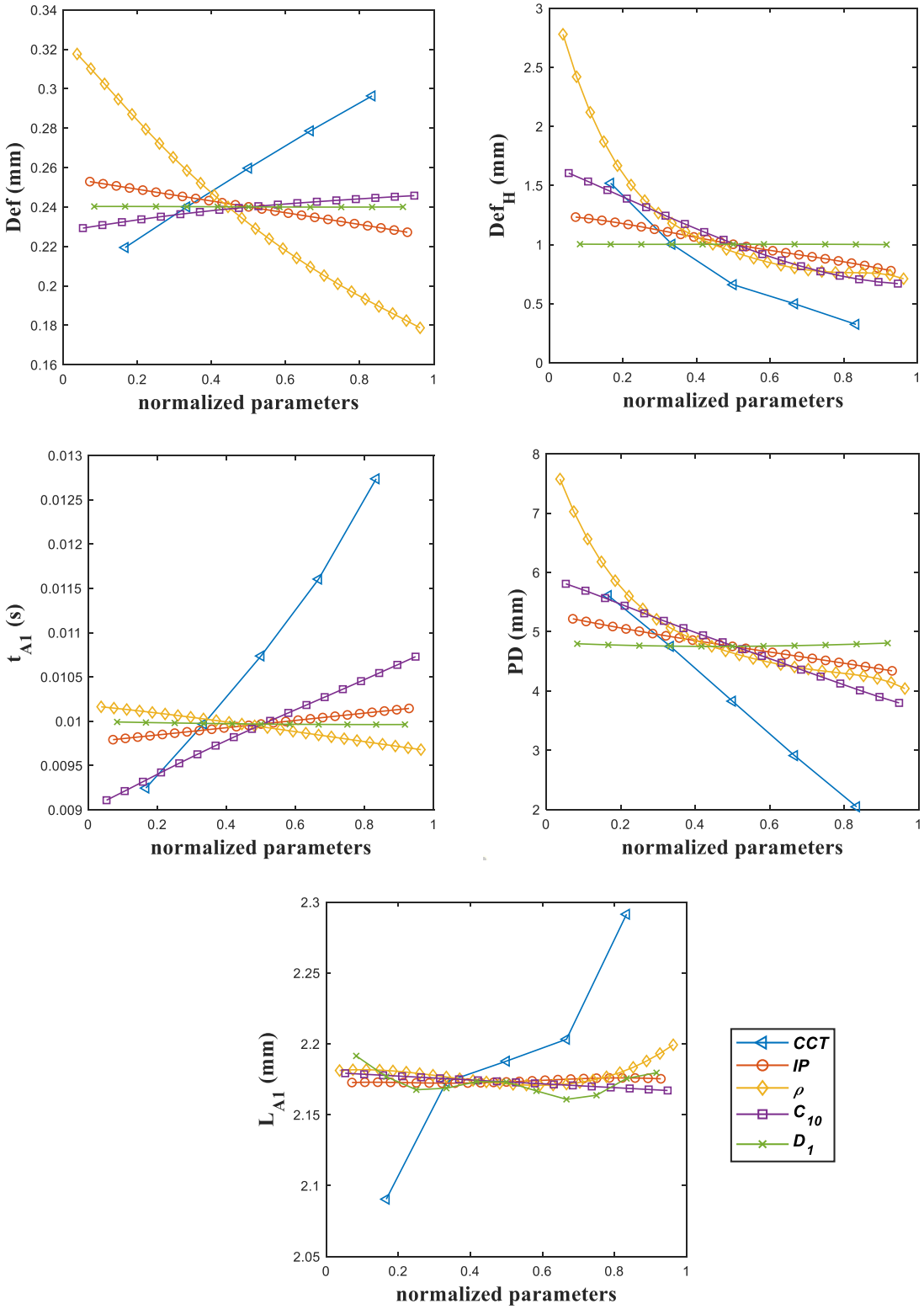

Fig. 12. Analysis of the effect of input parameter on the outputs.

reason for using the CorVis tonometer test is the valuable parameters that are evaluated during this process. There are many methods available today to calculate and modify the CVS_IOP. The impact of measurements from the statistical information and the numerical results of other studies can lead to further errors whereas, in this model, the factors affecting the measurements are known. Additionally, the transformation of the finite element model into a mathematical model makes it an appropriate model for real-time ophthalmic applications.

In this study, corneal geometry including thickness and curvature, corneal structural model, biomechanical properties, IOP, and corneal boundary conditions are determined, and CorVis tonometer parameters are calculated by simulating the CorVis tonometer. Then, by using

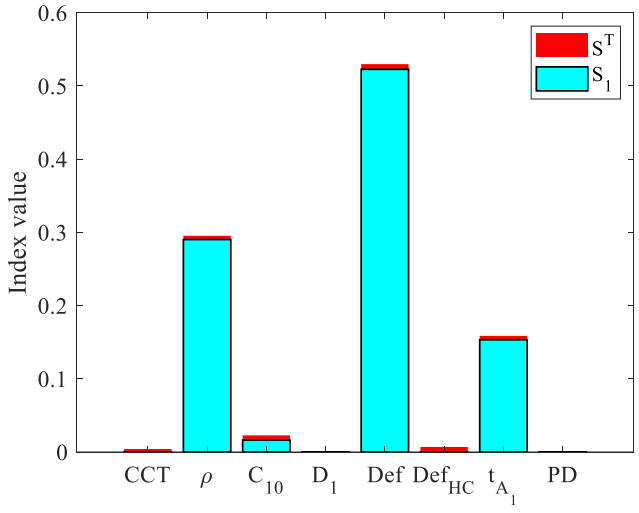

Fig. 13. Sobol sensitivity indices of the internal pressure.

adaptive-sparse PCE, we present a mathematical model of this simulation for each of the CorVis tonometer parameters. Afterward, using an inverse method, the IOP is obtained as a black box function of the geometrical parameters, material properties, and the CorVis tonometer parameters. Therefore, this model is capable of delivering IOP only with known or measurable parameters. Sobol indices of the initial and final mathematical models demonstrate that IOP is strongly correlated with deflection, first applanation time, and the radius of external curvature ρ.

These mathematical models are based on finite element models. Finite element models are also created using clinical data and evaluated using clinical results. On the other hand, the results of mathematical models are evaluated with the results of finite element models and, since they have very low cross-validation errors, they are highly reliable. Sensitivity analyses of these models prove that, in addition to the radius of curvature, some of the CorVis tonometer parameters including applanation time and corneal displacement until applanation time are very important in pressure measurement and can be used in other tonometers. The sensitivity analyses of Def and first applanation time show that, if the central corneal thickness, radius of curvature, or biomechanical properties are not properly simulated so the results are of poor accuracy.

CRediT authorship contribution statement

Vahid Yaghoubi: Writing – review & editing, Writing – original draft, Visualization, Supervision, Methodology, Investigation. **Hamed Setayeshnasab:** Writing – original draft, Software, Resources, Investigation. **Peiman Mosaddegh:** Writing – review & editing, Writing – original draft, Supervision, Software, Resources, Project administration, Methodology, Investigation, Conceptualization. **Mahmoud Kadkhodaei:** Writing – review & editing, Writing – original draft, Supervision, Project administration, Methodology, Investigation, Conceptualization.

Declaration of competing interest

The authors declare that they have no known competing financial interests or personal relationships that could have appeared to influence the work reported in this paper.

References

Ali, N.Q., Patel, D. v, McGhee, C.N.J., 2014. Biomechanical responses of healthy and keratoconic corneas measured using a noncontact scheimpflug-based tonometer. Investig. Ophthalmol. Vis. Sci. 55, 3651–3659.

Ambrósio, R., et al., 2011. Evaluation of corneal shape and biomechanics before LASIK. Int. Ophthalmol. Clin. 51, 11–38.

Asejczyk-Widlicka, M., Śródka, D.W., Kasprzak, H., Iskander, D.R., 2004. Influence of intraocular pressure on geometrical properties of a linear model of the eyeball: effect of optical self-adjustment. Optik 115, 517–524.

Bagheri, N.M., Kadkhodaei, M., Pirhadi, S., Mosaddegh, P., 2021. Effects of intracorneal ring segments implementation technique and design on corneal biomechanics and keratometry in a personalized computational analysis. Sci. Rep. 11, 1–24.

Bak-Nielsen, S., Pedersen, I.B., Ivarsen, A., Hjortdal, J., 2014. Dynamic Scheimpflug-based assessment of keratoconus and the effects of corneal cross-linking. J. Refract. Surg. 30, 408–414.

Bekesi, N., Dorronsoro, C., Hoz, A. de la, Marcos, S., 2016. Material properties from air puff corneal deformation by numerical simulations on model corneas. PLoS One 11, e0165669.

Blatman, G., Sudret, B., 2008. Sparse polynomial chaos expansions and adaptive stochastic finite elements using a regression approach. Compt. Rendus Mec. 336, 518–523.

Blatman, G., Sudret, B., 2011. Adaptive sparse polynomial chaos expansion based on least angle regression. J. Comput. Phys. 230, 2345–2367.

Broman, A.T., Congdon, N.G., Bandeen-Roche, K., Quigley, H.A., 2007. Influence of corneal structure, corneal responsiveness, and other ocular parameters on tonometric measurement of intraocular pressure. J. Glaucoma 16, 581–588.

Chihara, E., 2008. Assessment of true intraocular pressure: the gap between theory and practical data. Surv. Ophthalmol. 53, 203–218.

Cui, Y.-H., et al., 2015. Study on establishment and mechanics application of finite element model of bovine eye. BMC Ophthalmol. 15 (1 15), 1–16, 2015.

Dubbelman, M., Sicam, V., van der Heijde, G.L., 2006. The shape of the anterior and posterior surface of the aging human cornea. Vis. Res. 46, 993–1001.

Dupps Jr., W.J., Wilson, S.E., 2006. Biomechanics and wound healing in the cornea. Exp. Eye Res. 83, 709–720.

Ehlers, N., Bramsen, T., Sperling, S., 1975. Applanation tonometry and central corneal thickness. Acta Ophthalmol. 53, 34–43.

Eliasy, A., Chen, K.J., Vinciguerra, R., Maklad, O., Vinciguerra, P., Ambrósio Jr., R., Elsheikh, A., 2018. Ex-vivo experimental validation of biomechanically-corrected intraocular pressure measurements on human eyes using the CorVis ST. Exp. Eye Res. 175, 98–102.

Elsheikh, A., Alhasso, D., Gunvant, P., Garway-Heath, D., 2011. Multiparameter correction equation for Goldmann applanation tonometry. official publication of the American Academy of Optometry Optom. Vis. Sci. 88.

Fricker, T.E., Oakley, J.E., Sims, N.D., Worden, K., 2011. Probabilistic uncertainty analysis of an FRF of a structure using a Gaussian process emulator. Mech. Syst. Signal Process. 25, 2962–2975.

Frings, A., et al., 2015. Effects of laser in situ keratomileusis (LASIK) on corneal biomechanical measurements with the Corvis ST tonometer. Clin. Ophthalmol. 9, 305.

Ghanem, R., Spanos, P., 2003. Stochastic Finite Elements: a Spectral Approach. Courier Corporation.

Goldmann, H., 1955. Un nouveau tonometre d'applanation. Bull. Soc. Ophtalmol. Fr. 67, 474–478.

Han, Z., Sui, X., Zhou, D., Zhou, C., Ren, Q., 2013. Biomechanical and refractive behaviors of keratoconic cornea based on three-dimensional anisotropic hyperelastic models. J. Refract. Surg. 29, 282–290.

Harada, Y., Hirose, N., Kubota, T., Tawara, A., 2008. The influence of central corneal thickness and corneal curvature radius on the intraocular pressure as measured by different tonometers: noncontact and goldmann applanation tonometers. J. Glaucoma 17, 619–625.

Hassan, Z., Modis Jr., L., Szalai, E., Berta, A., Nemeth, G., 2014. Examination of ocular biomechanics with a new Scheimpflug technology after corneal refractive surgery. Contact Lens Anterior Eye 37, 337–341.

Hsu, S.Y., Chang, M.S., Lee, C.J., 2009. Intraocular pressure assessment in both eyes of the same patient after laser in situ keratomileusis. J. Cataract Refract. Surg. 35, 76–82.

Huseynova, T., Waring IV, G.O., Roberts, C., Krueger, R.R., Tomita, M., 2014. Corneal biomechanics as a function of intraocular pressure and pachymetry by dynamic infrared signal and Scheimpflug imaging analysis in normal eyes. Am. J. Ophthalmol. 157, 885–893.

Jannesari, M., Mosaddegh, P., Kadkhodaei, M., Kasprzak, H., Jabbarvand Behrouz, M., 2018a. Numerical and clinical investigation on the material model of the cornea in Corvis tonometry tests: differentiation between hyperelasticity and viscoelasticity, 3 23 Mech. Time-Dependent Mater. 23, 373–384, 2018.

Jannesari, M., Kadkhodaei, M., Mosaddegh, P., Kasprzak, H., Behrouz, M.J., 2018b. Assessment of corneal and fatty tissues biomechanical response in dynamic tonometry tests by using inverse models. Acta Bioeng. Biomech. 20.

Joda, A.A., Shervin, M.M.S., Kook, D., Elsheikh, A., 2015. Development and validation of a correction equation for CorVis tonometry. Comput. Methods Biomech. Biomed. Eng. 19, 943–953.

Kanngiesser, H.E., Kniestedt, C., Robert, Y.C.A., 2005. Dynamic contour tonometry: presentation of a new tonometer. J. Glaucoma 14, 344–350.

Kaufmann, C., Bachmann, L.M., Thiel, M.A., 2003. Intraocular pressure measurements using dynamic contour tonometry after laser in situ keratomileusis. Investig. Ophthalmol. Vis. Sci. 44, 3790–3794.

Kerautret, J., Colin, J., Touboul, D., Roberts, C., 2008. Biomechanical characteristics of the ectatic cornea. J. Cataract Refract. Surg. 34, 510–513.

Kirwan, C., O'Keefe, M., 2008. Corneal hysteresis using the Reichert ocular response analyser: findings pre- and post-LASIK and LASEK. Acta Ophthalmol. 86, 215–218.

Kohlhaas, M., et al., 2006. Effect of central corneal thickness, corneal curvature, and axial length on applanation tonometry. Arch. Ophthalmol. 124, 471–476.
Kwon, T.H., Ghaboussi, J., Pecknold, D.A., Hashash, Y.M., 2008. Effect of cornea material stiffness on measured intraocular pressure. J. Biomech. 41, 1707–1713.
Lee, R., et al., 2016. Novel parameter of corneal biomechanics that differentiate normals from glaucoma. J. Glaucoma 25, e603–e609.
Lee, H., et al., 2017. Changes in biomechanically corrected intraocular pressure and dynamic corneal response parameters before and after transepithelial photorefractive keratectomy and femtosecond laser–assisted laser in situ keratomileusis. J. Cataract Refract. Surg. 43, 1495–1503.
Liu, J., Roberts, C.J., 2005. Influence of corneal biomechanical properties on intraocular pressure measurement: quantitative analysis. J. Cataract Refract. Surg. 31, 146–155.
Lopes, B.T., et al., 2017. Repeatability and reproducibility of intraocular pressure and dynamic corneal response parameters assessed by the corvis ST. J. Ophthalmol. 2017.
Luce, D.A., 2005. Determining in vivo biomechanical properties of the cornea with an ocular response analyzer. J. Cataract Refract. Surg. 31, 156–162.
Marelli, S., Sudret, B., 2014. UQLab: a framework for uncertainty quantification in matlab. In: Vulnerability, Uncertainty, and Risk: Quantification, Mitigation, and Management, pp. 2554–2563.
Nemeth, G., et al., 2017. Corneal biomechanical data and biometric parameters measured with Scheimpflug-based devices on normal corneas. Int. J. Ophthalmol. 10, 217.
Nguyen, T., Boyce, B., 2011. An inverse finite element method for determining the anisotropic properties of the cornea. Biomech. Model. Mechanobiol. 10, 323–337.
Orssengo, G.J., Pye, D.C., 1999. Determination of the true intraocular pressure and modulus of elasticity of the human cornea in vivo, 3 61 Bull. Math. Biol. 61, 551–572, 1999.
Pedersen, I.B., Bak-Nielsen, S., Vestergaard, A.H., Ivarsen, A., Hjortdal, J., 2014. Corneal biomechanical properties after LASIK, ReLEx flex, and ReLEx smile by Scheimpflug-based dynamic tonometry. Graefe's Arch. Clin. Exp. Ophthalmol. 252, 1329–1335.
Rangarajan, N., et al., 2009. Finite element model of ocular injury in abusive head trauma. J. Am. Assoc. Pediatr. Ophthalmol. Strabismus 13, 364–369.
Romero-Jiménez, M., Santodomingo-Rubido, J., Wolffsohn, J.S., 2010. Keratoconus: a review. Contact Lens Anterior Eye 33, 157–166.
Schobi, R., Sudret, B., Wiart, J., 2015. POLYNOMIAL-CHAOS-BASED kriging. Int. J. Uncertain. Quantification 5, 171–193.
Schuëller, G.I., Pradlwarter, H.J., 2009. Uncertain linear systems in dynamics: retrospective and recent developments by stochastic approaches. Eng. Struct. 31, 2507–2517.
Schutte, S., van den Bedem, S.P.W., van Keulen, F., van der Helm, F.C.T., Simonsz, H.J., 2006. A finite-element analysis model of orbital biomechanics. Vis. Res. 46, 1724–1731.
Shah, S., Laiquzzaman, M., Bhojwani, R., Mantry, S., Cunliffe, I., 2007. Assessment of the biomechanical properties of the cornea with the ocular response analyzer in normal and keratoconic eyes. Investig. Ophthalmol. Vis. Sci. 48, 3026–3031.
Shen, Y., et al., 2014a. Comparison of corneal deformation parameters after SMILE, LASEK, and femtosecond laser-assisted LASIK. J. Refract. Surg. 30, 310–318.
Shen, Y., et al., 2014b. Changes in corneal deformation parameters after lenticule creation and extraction during small incision lenticule extraction (SMILE) procedure. PLoS One 9, e103893.
Singh, M., et al., 2016. Investigating elastic anisotropy of the porcine cornea as a function of intraocular pressure with optical coherence elastography. J. Refract. Surg. 32, 562–567.
Sinha Roy, A., Kurian, M., Matalia, H., Shetty, R., 2015. Air-puff associated quantification of non-linear biomechanical properties of the human cornea in vivo. J. Mech. Behav. Biomed. Mater. 48, 173–182.
Smedowski, A., Weglarz, B., Tarnawska, D., Kaarniranta, K., Wylegala, E., 2014. Comparison of three intraocular pressure measurement methods including biomechanical properties of the cornea. Investig. Ophthalmol. Vis. Sci. 55, 666–673.
Sobol, I., 1993. Sensitivity estimates for nonlinear mathematical models. Math. Model Civ. Eng. 407–414.
Sudret, B., 2008. Global sensitivity analysis using polynomial chaos expansions. Reliab. Eng. Syst. Saf. 93, 964–979.
Tian, L., et al., 2014. Assessment of ocular biomechanics using dynamic ultra high-speed Scheimpflug imaging in keratoconic and normal eyes. J. Refract. Surg. 30, 785–791.
Tian, L., et al., 2016. Corneal biomechanical characteristics measured by the CorVis Scheimpflug technology in eyes with primary open-angle glaucoma and normal eyes. Acta Ophthalmol. 94, e317–e324.
Vinciguerra, R., et al., 2016. Influence of pachymetry and intraocular pressure on dynamic corneal response parameters in healthy patients. J. Refract. Surg. 32, 550–561.
Whitford, C., Movchan, N.v., Studer, H., Elsheikh, A., 2017. A viscoelastic anisotropic hyperelastic constitutive model of the human cornea. Biomech. Model. Mechanobiol. 17, 19–29.
Yaghoubi, V., Marelli, S., Sudret, B., Abrahamsson, T., 2017. Sparse polynomial chaos expansions of frequency response functions using stochastic frequency transformation. Probabilist. Eng. Mech. 48, 39–58.
Ye, C., Yu, M., Lai, G., Jhanji, V., 2015. Variability of corneal deformation response in normal and keratoconic eyes. Optom. Vis. Sci. 92, e149–e153.